International Journal of Solids and Structures 49 (2012) 1103–1116

Contents lists available at SciVerse ScienceDirect

International Journal of Solids and Structures

journal homepage: www.elsevier.com/locate/ijsolstr

Static and dynamic response of elastic suspended cables with thermal effects

Marco Lepidi *, Vincenzo Gattulli

Dipartimento di Ingegneria delle Strutture, delle Acque e del Terreno, Università dell'Aquila, via G. Gronchi 18, 67100 L'Aquila, Italy

ARTICLE INFO

Article history:
Received 19 October 2011
Received in revised form 27 December 2011
Available online 2 February 2012

Keywords:
Cables
Temperature
Statics
Free dynamics
Frequency veering

ABSTRACT

Cable structures are often subjected to severe and variable environmental conditions, and their mechanical behavior is known to be particularly sensitive to different ambient factors. The paper analyzes temperature effects on the static and dynamic response of suspended inclined cables through a continuous monodimensional model including geometric nonlinearities. Uniform temperature changes are introduced through a non-homogeneous constitutive law for the material linear elasticity. Exact and approximate solutions of the equations governing the cable static equilibrium under self-weight are achieved, and the significance of the temperature-dependent variation of tension and sag are parametrically investigated. The spectral properties characterizing the free dynamics are obtained in a closed-form fashion for shallow parabolic cables within the low frequency vibration range. The sensitivity of the linear frequencies to temperature changes is discussed, outlining two thermal effects, which are distinguished by their different origins, geometric or static. For a generic temperature change, the geometric effect produces a systematic increment or reduction of all the frequencies, for both symmetric and anti-symmetric modes. The static effect stiffens or softens only the symmetric modes, and may prevail over the competing geometric effect, depending on the cable Irvine parameter. Finally, the thermal effects on the frequency veering and modal hybridization phenomena, which characterize quasi-resonant shallow cubic cables, are analyzed.

0. Introduction

Stay cables are widely employed in modern engineering due to their structural efficiency, economic affordability and architectural aesthetics. However, their characteristic slenderness and flexibility, combined with limited damping properties, expose structural cables to high-amplitude vibrations often generated by complex dynamic phenomena, including for instance modal localization (Gattulli and Lepidi, 2007), nonlinear interactions (Rega, 2004) and aerodynamic instabilities (Matsumoto et al., 1998). In addition, increasingly severe design requirements and challenging environmental conditions, together with recent advances in the material technology, are driving applied research oriented to understanding and improving cable performance in service conditions. Increasing attention is thus being devoted to cable structures in order to develop effective techniques for modal identification and model updating (Caetano et al., 2008), smart strategies of vibration control (Gattulli, 2007), non-destructive methods for early-detection of damage (Tabatabai, 2005) and new technologic solutions based on composite materials (Wang and Wu, 2010).

Despite rarely being approached in the available scientific literature, the temperature effect on the mechanical behavior of structural cables represents an issue of theoretical and practical interest, cutting across these different areas and levels of research. Indeed, experimental observations reveal that temperature changes can significantly affect the rich scenario of bifurcation phenomena characterizing the nonlinear behavior of laboratory prototypes (Rega and Alaggio, 2009), and may also disturb the operational modal analysis underlying many vibration-based procedures for the health monitoring of large-span, cable-stayed structures (Macdonald and Daniell, 2005; Degrauwe et al., 2009). Focusing on the second issue, temperature changes are known to significantly modify the natural frequencies and modal shapes whose variation is commonly selected as an indicator of structural damage. The consequent risk of false-positive or false-negative damage warnings may invalidate the entire diagnostic process.

On the other hand, the modern wireless networks deployed for structural health monitoring applications, composed of multi-sensor nodes, are increasing the potential to address the problem, providing access to a larger pool of measured information, including environmental variables. Therefore, the disturbances caused by thermal effects can be removed from damage identification procedures by developing suited parametric models of damage indicator sensitivity to varying temperature.

When long-term monitoring programs can be completed to populate a sufficiently rich database of experimental observations, including daily and seasonal variations, parametric models of the

* Corresponding author.
E-mail address: marco.lepidi@univaq.it (M. Lepidi).

0020-7683/$ - see front matter © 2012 Elsevier Ltd. All rights reserved.
doi:10.1016/j.ijsolstr.2012.01.008

frequency-temperature relation can be built up on empirical bases. According to different *black-box* correlation strategies, regression techniques can be employed to derive 'static' (i.e. time-independent) nonlinear formulas (Yang et al., 2010) or identify autoregressive linear 'dynamic' models (Peeters et al., 2001); otherwise, learning algorithms can be adopted to train binary classifiers (Ni et al., 2005) or neural networks (Zhou et al., 2010). Following a slightly different approach, experimental information from long term monitoring can be employed to characterize the environmental conditions as stochastic processes, and therefore to extract statistical models of the frequency-temperature relation, for instance using factor analysis (Deraemaeker et al., 2008). With respect to this framework, a completely different perspective is offered by deterministic models derived from direct thermo-mechanical formulations (Basseville et al., 2010). Though their realistic applications tend to be limited to simple structures, or even single structural elements, due to the inherent complexity of thermo-mechanical phenomena, deterministic models hold some advantages which may recommend their adoption as an alternative or addition to modern data-driven models. First, physical models can be generalized, as their reliability is not restricted to the particular structure on which they have been identified; moreover, a limited amount of experimental data is generally sufficient for their validation. Second, physical models may furnish a valuable mechanical interpretation of the structural behavior under thermal load, which in turn may contribute to an a priori recognition of the temperature signature on damage-sensitive structural features, and therefore to removing thermal effects from response-based structural health monitoring techniques.

Moving on from the arguments above, the paper presents a continuous mono-dimensional model of an inclined suspended cable, accounting for thermal effects in the material constitutive law (Section 1.1). Taking into account the axial elasticity, the static problem is solved in an analytically exact fashion, obtaining the cable equilibrium configuration under self-weight load and uniform quasi-static temperature change (Section 1.2). Next, a polynomial (parabolic or cubic) approximation of the static profile curve is introduced for shallow cables, accounting for thermal effects in an equivalent manner (Section 1.3). The thermal effects are parametrically investigated and discussed to furnish a physical interpretation of the analytical findings through comparison with the static configuration of the cable at the reference temperature (Section 1.4). Next, the dynamic problem governing the free undamped planar vibrations is approached, deriving the nonlinear integral–differential equation of motion governing the low-frequency dominant transversal motion (Section 2.1). A modal analysis is performed to study the small-amplitude vibration range (Section 2.2). Symmetric and antisymmetric modes are obtained through the closed-form solution of the modal problem for parabolic cables (Section 2.2.1). Hybrid modes are obtained instead from the numerical solution of the modal problem for cubic cables, when frequency veering occurs to avoid perfect internal resonance conditions (Section 2.2.2). The sensitivity of the linear modal properties to temperature changes is investigated, with focus on the different origin and relative importance of two different thermal effects which can affect the symmetric and anti-symmetric modes, depending on the cable Irvine parameter (Section 2.3). Finally, concluding remarks are drawn.

1. Static response of the suspended cable

1.1. Problem formulation

A monodimensional continuous model is formulated to describe the static response of an elastic suspended cable. Homogeneous and hyperelastic constitutive properties are assumed for the material. A perfectly-flexible transversal behavior is assumed; that is, the shear and flexural rigidity are considered negligible, and only uniform distributions of tensile stresses and extensional strains are admitted in the cable cross-section. The curvilinear abscissa s is used to span the total arc-length L_0 of the natural (stress-free) cable configuration $\mathcal{C}_0$ (Fig. 1a), attributed conventionally to the reference temperature T_0.

Since the model hypotheses allow only axial internal forces, everywhere tangential to the cable profile, searching the cable response under gravity loads consists in solving a geometric shape-finding problem, pursuing the unknown equilibrium configuration $\mathcal{C}_S$ in the vertical plane (Fig. 1c). The cable is considered to be hanging between fixed supports S_A and S_B, at different levels. The relative horizontal distance L is denoted as the cable *span*, while the segment joining the supports is denoted as the cable *chord*, inclined at angle ϑ from the horizontal (Fig. 1d). The configuration $\mathcal{C}_S$ is characterized by an ambient temperature T, different from T_0. Choosing the curvilinear abscissa s as the only independent variable, the Cartesian coordinate functions $x(s)$ and $y(s)$, which parametrically locate the position of each cable particle point $P(s)$ in the vertical plane, have to be determined. Additional unknown functions of interest are the curvilinear abscissa $p(s)$ spanning the strained static configuration $\mathcal{C}_S$, and the axial tension $N(s)$.

If only the static effects of cable self-weight are considered, the cable wholly lies in the vertical plane, so that the following geometric constraint must be satisfied

$$\left(\frac{\mathrm{d}x}{\mathrm{d}p}\right)^2+\left(\frac{\mathrm{d}y}{\mathrm{d}p}\right)^2=1 \tag{1}$$

At the same time, considering constant weight per unit natural length w, the global equilibrium of the left-hand cable region with respect to the current point $P(s)$, requires that

$$N\frac{\mathrm{d}x}{\mathrm{d}p}=H,\quad N\frac{\mathrm{d}y}{\mathrm{d}p}=V-ws \tag{2}$$

where H and V are the unknown vertical and horizontal S_A support reactions, respectively (Fig. 1b).

Adopting an exact kinematic formulation, linear elasticity of the material, and temperature-independent Young modulus E, the constitutive relation reads

$$N=EA\left(\frac{\mathrm{d}p}{\mathrm{d}s}-1-\alpha\Delta T\right) \tag{3}$$

where A is the undeformed area of the cable cross-section. The right-hand term represents the elastic part of the lagrangian extensional strain, once purged of the thermal contribution linearly depending on the uniform temperature change $\Delta T=T-T_0$, given the thermal expansion coefficient α.

Having fixed the origin of the coordinate functions $x(s)$ and $y(s)$ at the left support, the geometric boundary conditions at S_A ($s=0$) and S_B ($s=L_0$) read

$$x(0)=0,\quad y(0)=0,\quad x(L_0)=L,\quad y(L_0)=L\tan(\vartheta) \tag{4}$$

and the special case of leveled supports (*horizontal cables*) can be considered setting $\vartheta=0$.

1.2. Exact solution

The solution strategy for the static problem follows the direct force method, in which the support reactions H and V are assumed as principal unknowns. In virtue of the geometric constraint (1), squaring each of the equilibrium conditions (2), and adding the resulting expressions, the axial tension reads

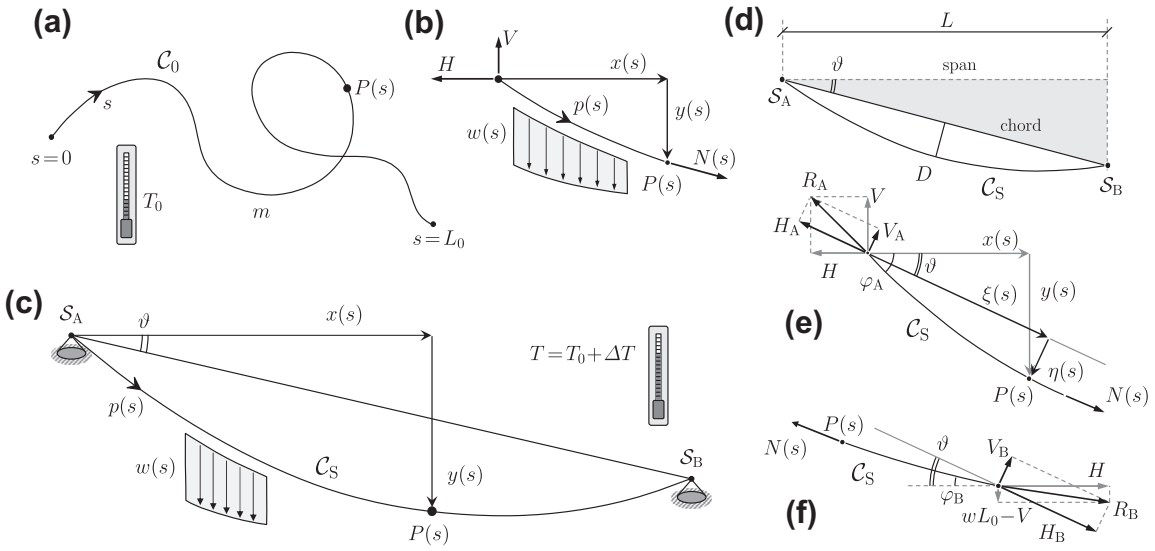

Fig. 1. Static response of the suspended cable under self-weight: (a) natural unstressed configuration $\mathcal{C}_0$, (b) global static equilibrium, (c) static equilibrium configuration $\mathcal{C}_S$, (d) cable span and inclined chord and (e), (f) alternative coordinates and reactions at the supports.

$$N(s) = \left[H^2 + (V - ws)^2\right]^{\frac{1}{2}} \tag{5}$$

where the contribution of the horizontal component $N_x = H$, which is everywhere constant due to the absence of horizontal loads, can be distinguished from the s-dependent vertical one $N_y(s) = (V - ws)$.

Therefore, applying the chain rule to the derivatives in Eq. (2), imposing the constitutive relation (3) into the resulting expressions, a couple of nonlinear, first order, ordinary differential equations in the principal unknowns $x(s)$ and $y(s)$ is obtained. Using the solution (5) for the cable tension $N(s)$, the equations can be handled for symbolic integration, so that imposing the boundary conditions (4a and b) leads to the closed form solution

$$\begin{aligned} x(s) &= \frac{H}{EA}s + \frac{H}{w}(1+\alpha\Delta T)\Psi_1(s), \quad y(s) \\ &= \frac{V}{EA}s - \frac{1}{2}\frac{w}{EA}s^2 + \frac{H}{w}(1+\alpha\Delta T)\Psi_2(s) \end{aligned} \tag{6}$$

where the nondimensional auxiliary functions $\Psi_1(s)$ and $\Psi_2(s)$, which only depend on the support reactions, are reported in the Appendix. According to the force method strategy, the remaining geometric boundary conditions (4c and d), imposed on the solution, furnish a pair of compatibility equations

$$\begin{aligned} &\frac{HL_0}{EA} + \frac{H}{w}(1+\alpha\Delta T)\Psi_1(L_0) = L, \\ &\frac{VL_0}{EA} - \frac{1}{2}\frac{wL_0^2}{EA} + \frac{H}{w}(1+\alpha\Delta T)\Psi_2(L_0) = L\tan(\vartheta) \end{aligned} \tag{7}$$

which have to be solved to determine the unknown support reactions H and V. In the particular case of horizontal cables, due to the zeroing of the right-hand part, the second equation is identically satisfied by the solution $V = wL_0/2$, and the first equation is sufficient to determine the remaining unknown H.

From a geometrical viewpoint, the cable equilibrium configuration $\mathcal{C}_S$ is exactly described by a *parametric planar curve*, whose map from the s-parameter domain to the vertical plane is defined by the coordinate functions $x(s)$ and $y(s)$. Since this curve results from the exact solution of the equations governing the cable static response, taking into account the axial elasticity, it is traditionally referred to as the *exact elastic catenary* (Irvine, 1981), here modified to account for thermal effects.

A closed form solution can also be obtained for the curvilinear abscissa $p(s)$ of the strained static configuration $\mathcal{C}_S$, by integrating the Eq. (3)

$$p(s) = (1+\alpha\Delta T)s + \frac{1}{2w}\frac{H^2}{EA}[\Psi_3(s) + \Psi_4(s)] \tag{8}$$

where the auxiliary functions $\Psi_3(s)$ and $\Psi_4(s)$ are reported in the Appendix. Moreover, differentiating the function $p(s)$ and subtracting unity, the s-distribution of the cable axial extensional strain is obtained.

To generalize the comments on the static problem solution for each cable inclination, it is convenient to replace the *global coordinate* functions $x(s)$ and $y(s)$ with the *local coordinate* functions $\xi(s)$ and $\eta(s)$, referred to a pair of inclined axes, tangent and normal to the cable chord, respectively (Fig. 1e and f). Coherently, the support reactions R_A and R_B can be decomposed in the local components

$$\begin{aligned} H_A &= H\cos(\vartheta) + V\sin(\vartheta), \\ V_A &= V\cos(\vartheta) - H\sin(\vartheta) \end{aligned} \tag{9}$$

$$\begin{aligned} H_B &= H\cos(\vartheta) + (wL_0 - V)\sin(\vartheta), \\ V_B &= H\sin(\vartheta) - (wL_0 - V)\cos(\vartheta) \end{aligned} \tag{10}$$

while the cable particle point $P(s)$ is located in the vertical plane by the local coordinate functions

$$\begin{aligned} \xi(s) &= \frac{x(s)}{\cos(\vartheta)} + [y(s) - x(s)\tan(\vartheta)]\sin(\vartheta), \quad \eta(s) \\ &= [y(s) - x(s)\tan(\vartheta)]\cos(\vartheta) \end{aligned} \tag{11}$$

and the coordinates of the left-hand support becomes $\xi = L/\cos(\vartheta)$ and $\eta = 0$.

The solution sensitivity to varying mechanical properties can be assessed by parametric analyses. To this end, it is convenient to introduce a pair of independent nondimensional parameters, originally proposed by Irvine and Sinclair (1976) to synthetically characterize the cable elasto-geometrical properties

$$\varrho = \frac{wL_0}{2EA}, \quad \Lambda = \frac{L_0}{L}\cos(\vartheta). \tag{12}$$

Since ϱ represents the static elongation experienced by a half-length fixed-free cable with axial stiffness EA, hanging vertically under its self-weight, it is referred to as the cable *flexibility factor*. The wholly-geometric Λ parameter, which is known as the cable *aspect*

ratio, represents instead the ratio between the natural cable length and the distance between the supports, and also allows a distinction between statically pretensioned ($\Lambda < 1$) and non-pretensioned ($\Lambda > 1$) cables.

The static problem solution can be re-written in a proper non-dimensional form defining the following variables and quantities

$$\tilde{s} = \frac{s}{L_0}, \quad \tilde{x} = \frac{x}{L}, \quad \tilde{y} = \frac{y}{L}, \quad h = \frac{2H}{wL_0}, \quad v = \frac{2V}{wL_0}, \quad \tilde{\xi} = \frac{\xi}{L}\cos(\vartheta), \quad \tilde{\eta} = \frac{\eta}{L}\cos(\vartheta). \tag{13}$$

Therefore, omitting the tilde to simplify the notation, the nondimensional coordinate functions read

$$x(s) = \frac{h\Lambda}{2\cos(\vartheta)}[2\varrho s + (1+\alpha\Delta T)\Psi_1(s)], \quad y(s) = \frac{\Lambda}{2\cos(\vartheta)}[2\varrho s(v-s) + h(1+\alpha\Delta T)\Psi_2(s)] \tag{14}$$

and the equations

$$h\Lambda[2\varrho + (1+\alpha\Delta T)\Psi_1(1)] = 2\cos(\vartheta), \quad \Lambda[2\varrho(v-1) + h(1+\alpha\Delta T)\Psi_2(1)] = 2\sin(\vartheta) \tag{15}$$

determine the unknown nondimensional reactions h and v. Finally, the coordinate change rules become

$$\xi(s) = x(s)\cos^2(\vartheta) + y(s)\sin(\vartheta)\cos(\vartheta), \quad \eta(s) = y(s)\cos^2(\vartheta) - x(s)\sin(\vartheta)\cos(\vartheta) \tag{16}$$

and the nondimensional coordinates at the left-hand support ($s = 1$) are $\xi = 1$ and $\eta = 0$.

A notable nondimensional quantity, often employed as a synthetic descriptor of the static problem solution in many theoretical formulations and technical applications for inclined cables, is the *sag-to-chord ratio*. The cable *sag* D is the chord-to-profile distance, measured at half of the distance between the supports (midchord), corresponding to the function $\eta(s)$ evaluated at the midchord natural abscissa s_c (Fig. 1d). Consequently, the *sag-to-chord ratio* $\delta = D/L\cos(\vartheta)$ reads, in nondimensional form

$$\delta = \frac{\Lambda}{2}[2(v\cos(\vartheta) - h\sin(\vartheta))\varrho s_c - \varrho\cos(\vartheta)s_c^2 + h(\Psi_2(s_c)\cos(\vartheta) - \Psi_1(s_c)\sin(\vartheta))] \tag{17}$$

where the natural abscissa s_c is determined from the nonlinear equation

$$2\Lambda\varrho(h\cos(\vartheta) + v\sin(\vartheta))s_c - 2\Lambda\varrho s_c\sin(\vartheta) + h\Lambda(\Psi_1(s_c)\cos(\vartheta) + \Psi_2(s_c)\sin(\vartheta)) = 1 \tag{18}$$

whose exact solution for horizontal cables is $s_c = 1/2$ for symmetry reasons.

1.3. Approximate solution

From a mathematical viewpoint, the elastic catenary curve resulting from the exact solution of the static problem tends to be difficult to handle, essentially due to the parametric form of the coordinate functions. Thus in many engineering applications minor approximations may be acceptable to greatly simplify the formulation and solution of nonlinear dynamic problems in which the static equilibrium profile is used as reference configuration. According to this general criterion, the static problem can be increasingly simplified as stronger hypotheses are successively introduced in the governing equations. Following a classic qualitative nomenclature based on the cable shallowness, the static profile of *moderately nonshallow* cables is described by the (non-elastic) catenary curve, obtained introducing the hypothesis of axial inextensibility. The flat profile of *shallow* cables is described instead by polynomial curves, obtained adding the hypothesis of closeness between the profile and the chord. As major significant results (Irvine and Caughey, 1974; Lacarbonara et al., 2007), these approximations make possible a closed-form solution of the modal problem which emerges from the linearized equations governing the small-amplitude free undamped oscillations in the low-frequency range of the cable transversal dynamics.

For the purposes of the present work, any approximation has to account for both the elastic and inelastic cable deformation. In particular, the smallness of the flexibility factor is no more sufficient to justify the traditional inextensibility hypothesis. Nonetheless, the simplifying hypothesis of uniform, though unknown, extensional strain associated to uniform temperature changes is sufficient to assume constant self-weight w_p per unit *strained* length. Handling the global equilibrium Eq. (2) according to this hypothesis and introducing the auxiliary function $z(x) = y(x) - x\tan(\vartheta)$ to measure the dip of the profile below the chord, the cable vertical equilibrium is governed by the nonlinear differential equation

$$H\frac{d^2z}{dx^2} = -w_p\left[1 + \left(\tan(\vartheta) + \frac{dz}{dx}\right)^2\right]^{\frac{1}{2}} \tag{19}$$

equipped with homogeneous boundary conditions. Reducing the static problem to a single equilibrium equation requires that some of the unknowns must be specified beforehand. Namely, it is necessary to assess a priori the two constant coefficients, represented by the horizontal component of the axial tension and the weight density per unit strained length, depending on the extensional strain.

Considering only cables hanging closely to the chord, the problem statement can be further simplified. Analytically, the closeness between the static profile and the chord entails $dz = \epsilon dx$, where ϵ is a small parameter ($\epsilon \ll 1$). Therefore, the first order derivative in Eq. (19) can be considered sufficiently small with respect to unity for its square to be neglected. Expanding in ϵ-orders and retaining only terms up to the ϵ-power, a linear differential equation is obtained (Irvine, 1981)

$$H\frac{d^2z}{dx^2} + \epsilon w_p\frac{dz}{dx}\sin(\vartheta) = -\frac{w_p}{\cos(\vartheta)} \tag{20}$$

where the first order derivative can be considered a perturbation, due to the small coefficient. A nondimensional form of the dependent variable $\tilde{z} = z/L$ can be adopted, and the equation can be tackled employing a classic perturbation scheme. Expanding in ϵ–powers the nondimensional variable $\tilde{z} = \tilde{z}_0 + \epsilon\tilde{z}_1 + \mathcal{O}(\epsilon^2)$, substituting and collecting like terms, a hierarchy of second-order non-homogeneous equations is obtained. Solving each equation for homogeneous boundary conditions, the reconstructed solution reads

$$z(x) = \frac{4\delta_p}{\cos^2(\vartheta)}x(1-x)\left[1 + \frac{2\delta_p}{3\cos^2(\vartheta)}(1-2x)\sin(2\vartheta)\right], \quad \delta_p = \frac{w_pL}{8H}\cos(\vartheta) \tag{21}$$

where the tilde has been again omitted for sake of simplicity. According to the nondimensional coordinate change rule $\xi = x + \epsilon z\sin(\vartheta)\cos(\vartheta)$ and $\eta = z\cos^2(\vartheta)$, the solution can be expressed in local coordinates

$$\eta(\xi) = 4\delta_p\xi(1-\xi)\left[1 - \frac{8}{3}\delta_p(1-2\xi)\tan(\vartheta)\right] \tag{22}$$

where, applying the coordinate change, terms higher than $\mathcal{O}(\epsilon^2)$ have been neglected for consistency. It is worth noting that the nondimensional parameter δ_p represents the approximated

sag-to-chord ratio, as it corresponds to the value attained by the perturbation solution $\eta(\xi)$ at midchord.

Some qualitative remarks can be made, while further details on the approximated problem statement, supported by a discussion of the approximation validity of the first-order solution, can be found in Lepidi and Gattulli (2011). The perturbation solution describes the static equilibrium cable profile through the cubic function (22), in which the cubic term, depending on the squared sag-to-chord ratio, is a small (ϵ-order) correction of the quadratic generating solution. Therefore, shallow cables will be distinguished as *parabolic* or *cubic cables* in the following, depending on whether the sag-to-chord ratio makes the cubic term negligible or not. However, since the cubic term vanishes for leveled supports ($\vartheta = 0$), shallow horizontal cables can be rigorously classified as parabolic (at least within the validity range of the perturbation solution, that is, approximately for $\delta_p < 1/8$). On the other hand, shallow inclined cables can be classified either as parabolic or cubic. From a physical viewpoint, the chord inclination determines a slight perturbation of the parabolic profile valid for horizontal cables. This perturbation does not modify the midspan sag (as the cubic term zeroes at midchord), but is nonetheless sufficient to destroy the profile symmetry.

The equilibrium Eq. (20) is not sufficient by itself to govern the cable static problem, unless "the static effects of cable elasticity have already been accounted for in the determination of the tension and sag" (Irvine and Caughey, 1974). In fact, the solution (21)a is undetermined as long as the sag δ_p remains unassessed. In virtue of the relation (21)b, the a posteriori assessment of the sag is equivalent to the a priori assignment of the tension H and the weight w_p in the equilibrium equation. In other words, the relation (21)b establishes a constraint among these three quantities, only two of which are independent free parameters. For the purpose of the present work, it is convenient to assign the tension H and the sag δ_p, forcing them to assume the values of the elastic catenary solution ($\delta_p = \delta$). This strategy is justified by the search for a satisfying geometric approximation of the available exact solution, whereas a second, approximate solution of the static problem would be redundant. In this respect, the leading idea (already sketched in exercise 2.5 of the Irvine book (Irvine, 1981)) is that any uniform change in the ambient temperature can be artfully described as an equivalent increment (or decrement) of the cable self-weight.

The approximate static solution is strongly characterized by a notable nondimensional quantity, known as the *Irvine parameter*, which synthetically accounts for the material elastic properties, the geometric stiffness and the shape of the static equilibrium profile. According to its original formulation (Irvine, 1981), the general form of the Irvine parameter for inclined cables is

$$\lambda^2 = \frac{EA}{H_*}\left(\frac{w_* L_*}{H_*}\right)^2 \frac{L_*}{L_{e*}} \tag{23}$$

where $w_* = w_p \cos(\vartheta)$, $H_* = H/\cos(\vartheta)$ and $L_* = L/\cos(\vartheta)$, whereas the auxiliary length L_{e*} is

$$L_{e*} = \int_0^{L_*} \left(\frac{dp}{d\xi}\right)^3 d\xi \tag{24}$$

and can be approximated, to the first significant ϵ-power, as $L_{e*} \simeq L_*(1 + 8\delta_p^2)$. Alternately, the Irvine parameter is traditionally presented in the form

$$\lambda^2 = 64\mu\delta_p^2 \Lambda_e \tag{25}$$

where $\mu = EA/H_*$ expresses the ratio between the axial elastic and the geometric transversal stiffness, and $\Lambda_e = L_*/L_{e*}$, which is usually close to unity, plays the role of a small reducing factor. It is useful to recall that the Irvine parameter is a monotonically increasing function of the aspect ratio Λ. In particular, the threshold $\Lambda = 1$, which separates the pretensioned and non-pretensioned cable range, can be proved to correspond to the critical value $\lambda_c^2 \simeq 24$ (Rega et al., 1984).

1.4. Effects of temperature changes

The present model can be easily verified to degenerate into the Irvine model (Irvine, 1981) for vanishing values of the temperature change. Therefore, the thermal effects can be discussed simply evidencing how the temperature modifies the Irvine solution, taken as reference. The essential temperature effects on the (exact) static equilibrium configuration can be globally captured by a pair of synthetic parameters

$$\chi^2 = \frac{H}{H_0}, \quad \kappa^2 = \frac{D}{D_0} \tag{26}$$

expressing the ratio between the different values assumed at the current and the reference (subscript 0) temperature by two relevant quantities, namely the horizontal tension H and the sag D. Therefore, the two parameters can be referred to as the *tension variation factor* χ^2, and the *sag variation factor* κ^2, respectively. Since in the large displacement field the cable transversal stiffness is furnished only by the geometric contribution due to the axial tension, the static sag naturally increases (or decreases) for negative (or positive) tension variations. Therefore it can be expected that the two factors χ^2 and κ^2 are not completely independent of each other. On the other hand, it could be demonstrated that they are totally dependent on each other ($\chi^2\kappa^2 = 1$) only in the limiting case of taut strings ($\Lambda \ll 1$). Note that the use of partially-dependent descriptors of the temperature effects is here justified by reasons of convenience, as will be better clarified in the statement of the dynamic problem.

Parametric analyses show how the tension and sag variation depend on the aspect ratio Λ, spanning a wide range including pretensioned ($\Lambda < 1$, or $\lambda^2 < \lambda_c^2$) and non-pretensioned cables ($\Lambda > 1$, or $\lambda^2 > \lambda_c^2$), for six different values of the temperature change (Fig. 2). The results refer to both horizontal (Fig. 2a and b) and inclined cables (Fig. 2c and d), with technically-significant values of the flexibility factor ($\varrho = 2 \times 10^{-5}$) and the thermal expansion coefficient ($\alpha = 10^{-5}$). Starting from a phenomenological viewpoint, it is immediately evident that a temperature increment (*warming*) determines a tension reduction ($\chi^2 < 1$) and a simultaneous sag augmentation ($\kappa^2 > 1$) in the whole Λ-range. On the contrary, a temperature decrement (*cooling*) determines opposite results. Such systematic trend agrees with the physical expectation that, warming up the environmental temperature, the suspended cable undergoes a partial relaxation of the internal forces and a simultaneous amplification of the static response. Moving to more specific aspects, it can be noted that, due to the reciprocal dependence of the two parameters, the κ^2-curves (Fig. 2b) and the χ^2-curves (Fig. 2a) exhibit a behavior qualitatively similar, though opposite in sign. Therefore the temperature effects can be summarized in a few points, looking mainly at the tension variation

i. fixing a certain aspect ratio Λ, which corresponds to selecting a particular cable, increasing (or decreasing) temperature changes proportionally reduce (or augment) the cable tension, even if not linearly. A minor remark is that tension variations due to equal warming and cooling action are also not perfectly symmetric with respect to the reference temperature (marked by $\chi^2 = 1$),
ii. fixing a certain temperature change ΔT, the corresponding χ^2-curve is not-monotonically dependent on the aspect ratio. Positive (or negative) temperature changes determine an absolute minimum (or maximum) of the tension

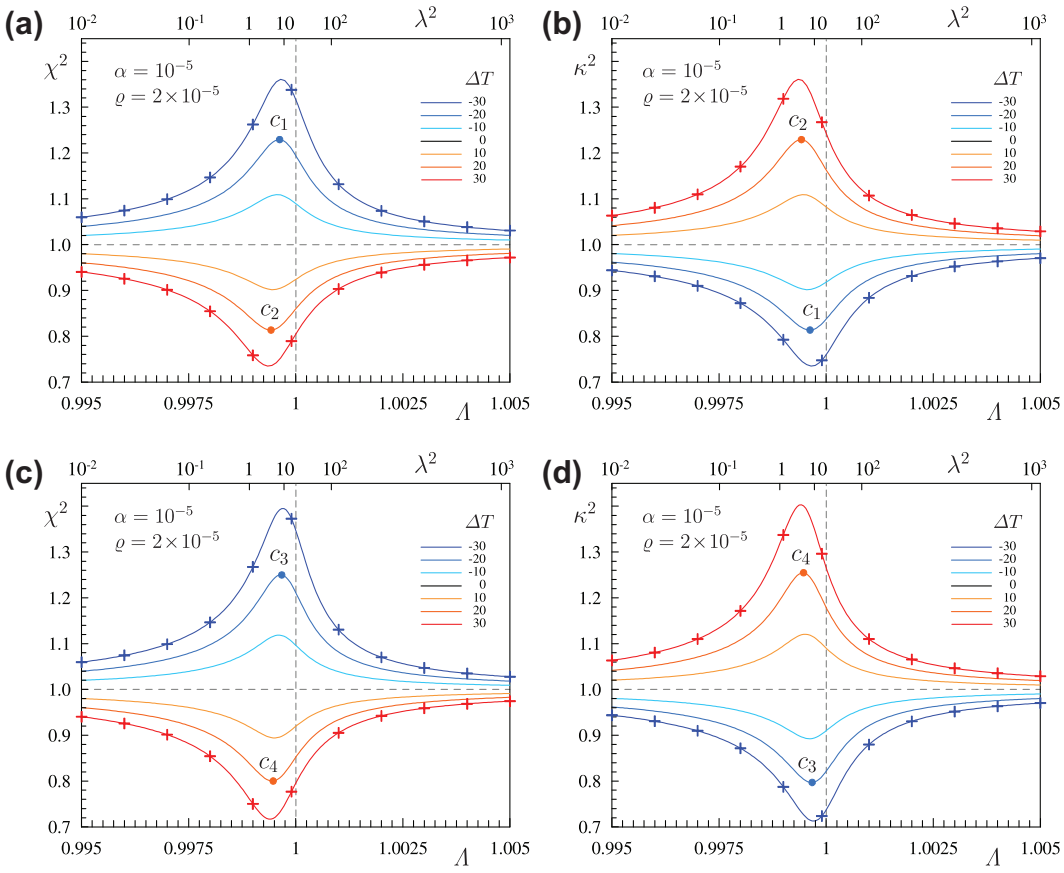

Fig. 2. Effect of different temperature changes on the synthetic descriptors of the static response for (a), (b) horizontal ($\vartheta = 0$) and (c), (d) inclined ($\vartheta = \pi/6$) suspended cables. Crosses mark finite element results.

variation, close to the transition value $\Lambda = 1$. For the limiting (highest or lowest) Λ-values, the curves develop horizontal asymptotes. The asymptotic χ^2-values are different from each other and from unity. A minor remark is that the maximum or minimum point slowly moves toward higher aspect ratios for decreasing temperature changes.

A finite element model has been formulated to verify these findings. The cable natural length has been divided into one hundred prestressed two-node truss elements. Then the nonlinear static problem has been solved in the framework of a software program package for thermo-dynamic incremental analyses (R&D ADINA, 2009), employing a large-displacement kinematic formulation to achieve the equilibrium configuration under self-weight and quasi-statically varying environment temperature. The finite element solutions (marked by the crosses in Fig. 2) confirm the analytical results with fine approximation.

A physical interpretation of the analysis results indicates that cables may exhibit a different sensitivity to temperature changes, depending on their aspect ratio or, equivalently, on their Irvine parameter. The highest sensitivity is shown by cables whose natural length is close to the distance between the supports ($\Lambda \simeq 1$). Cables of longer or shorter natural length become gradually less sensitive to thermal effects. Therefore, strongly pretensioned ($\Lambda \ll 1$) or non-pretensioned cables ($\Lambda \gg 1$) tend to exhibit a significantly lower, even if never null, temperature sensitivity. However, from a comparison, thermal effects on strongly pretensioned cables are quantitatively more important with respect to non-pretensioned cables.

Additional parametric results, here not reported for sake of conciseness, can be briefly summarized to better justify the different sensitivities to temperature changes, depending on the cable aspect ratio. At a certain temperature, the cable static tension monotonically decreases for increasing aspect ratios, but its reduction rate is strongly different for pretensioned (higher rate) and non-pretensioned (lower rate) cables. The transition, around $\Lambda = 1$, features a smooth but rapid rate change. Applying a positive (or negative) temperature change, the tension-to-aspect ratio dependence remains essentially unchanged, except for a translation to higher (or lower) aspect ratios. Since the two parameters χ^2 and κ^2 express the relative ratio of the tension and sag with respect to the reference temperature, it is immediately verified that the change-in-rate is responsible for the maximum (or minimum) of the parameter curves and the temperature change amplitude for the maximum position.

From a technical viewpoint, it might seem attractive to quickly account for the temperature effects on a particular cable, for instance by defining an equivalent value of the aspect ratio Λ. According to this idea, the natural cable length should be artfully modified to someway compensate for the inelastic deformation due to the assigned temperature change. Nonetheless, it can be proved that this adjustment is impossible working on the natural length only, because the equivalent modification of the aspect ratio would require at least a simultaneous compensation for the cable self-weight linear density. In other words, the static response of a cable undergoing an assigned temperature change is never identical to that of the *same* cable at the reference temperature, even if it supposed to be shortened or lengthened. On the

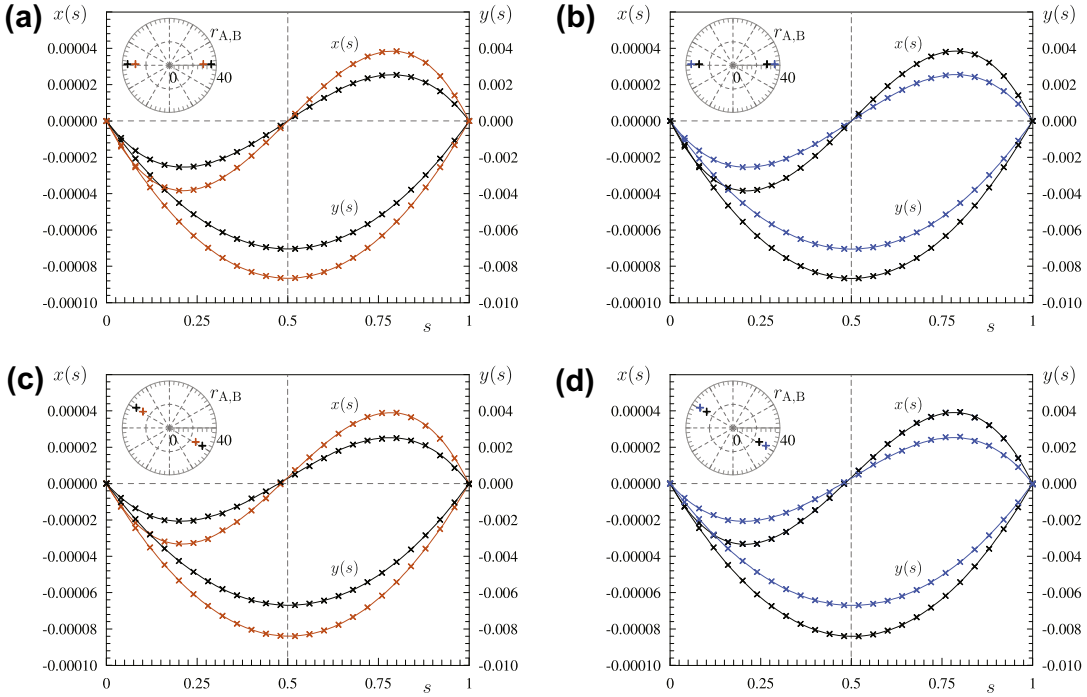

Fig. 3. Modification of the coordinate functions describing the static configuration $\mathcal{C}_S$ at the reference temperature (black), due to positive (red) or negative (blue) temperature changes $\Delta T = \pm 20$ for highly-sensitive cables: (a), (b) horizontal cables c_1 and c_2; (c), (d) inclined cables c_3 and c_4. Crosses mark finite element results. (For interpretation of the references to colour in this figure legend, the reader is referred to the web version of this article.)

other hand, the possibility that the temperature effects might be simulated through the static response of a *different* cable at the reference temperature turns out to have limited technical significance.

Fig. 3 illustrates how the global coordinate functions $x(s)$ and $y(s)$ are modified by the temperature change $\Delta T = \pm 20$. Fig. 3a and b refer to the horizontal cable with the highest sensitivity to the warming (the χ^2-maximum and the κ^2-minimum marked by the point c_1 in Fig. 2a and b) or cooling (point c_2). The increment or reduction of the function amplitude is evident, whereas the slight modification of the function shape, due to changes in the auxiliary functions $\Psi_1(s)$ and $\Psi_2(s)$, is not visually appreciable. Finally, the temperature change preserves the symmetry or antisymmetry featuring the two functions. For completeness, the polar plot on the top-left corner illustrates the modification (amplitude and direction) of the support reactions. Fig. 3c and d instead refer to the inclined cable with the highest sensitivity to the warming or cooling (points c_3 and c_4 in Fig. 2c and d). The effects of the temperature change are qualitatively and quantitatively similar to those affecting the horizontal cables. A significant difference, despite being hardly appreciable, is that positive (negative) temperature changes may increase (decrease) the slight asymmetry characterizing the coordinate functions of inclined cables. Again, finite element results, marked by the crosses, confirm with fine agreement the analytical finding.

A few qualitative remarks concerning the influence of the remaining mechanical properties, emerging from further parametric analyses extensively reported in Lepidi and Gattulli (2011), can be summarized. In particular, it is worth noting that cables with smaller flexibility factors ϱ (lighter, or axially stiffer cables) exhibit higher sensitivity to temperature. The ϱ-reduction determines a systematic amplification of the tension and the sag variation in almost the whole Λ-range. In particular, for positive (negative) temperature changes, the minimum (maximum) of the χ^2-factor is amplified and simultaneously moved towards the critical value $\Lambda = 1$, whereas the asymptotes corresponding to limiting Λ-values remain practically unaltered.

2. Dynamic response of the suspended cable

2.1. Problem formulation

The dynamic problem is formulated following the Irvine scheme (Irvine, 1981) to derive the equations of motion governing the in-plane vibrations of suspended elastic cables, with generic chord inclination. Under the assumption of quasi-static temperature changes, the cable configuration $\mathcal{C}_S$, known from the static problem solution and conveniently mapped by the local coordinate function $\eta(\xi)$, can be taken as initial fixed reference for the cable dynamic response. For the dynamic problem formulation, it does not matter whether the function $\eta(\xi)$ represents the exact elastic catenary solution, undergoing a suited ξ-reparametrization, or its polynomial approximation for shallow cables, sufficiently accurate if the static variables satisfy the ordering $\xi = \mathcal{O}(1)$, $\eta = \mathcal{O}(\epsilon)$, where ϵ is a small parameter ($\epsilon \ll 1$).

The dynamic configuration $\mathcal{C}_D$ at the same temperature T, spanned by the arc-length abscissa $c(\xi, t)$, is described in the vertical plane by the dimensional components of motion $u(\xi, t)$ and $v(\xi, t)$, oriented according to the local coordinate system (Fig. 4). When the simplifying hypothesis of shallow cables is introduced in the following, the dynamic variables will be ordered according to $u = \mathcal{O}(\epsilon^2)$ and $v = \mathcal{O}(\epsilon)$, and referred to as the *longitudinal* and *transversal* components of motion, respectively. From a physical viewpoint, recalling also the simultaneous assumptions for the static variables, this ordering postulates that the planar dynamics of shallow cables is dominated by transversal oscillations, whose amplitude is however insufficient to overcome the static sag.

The equations governing the cable dynamic equilibrium ensue from the virtual work principle, applied to the internal and

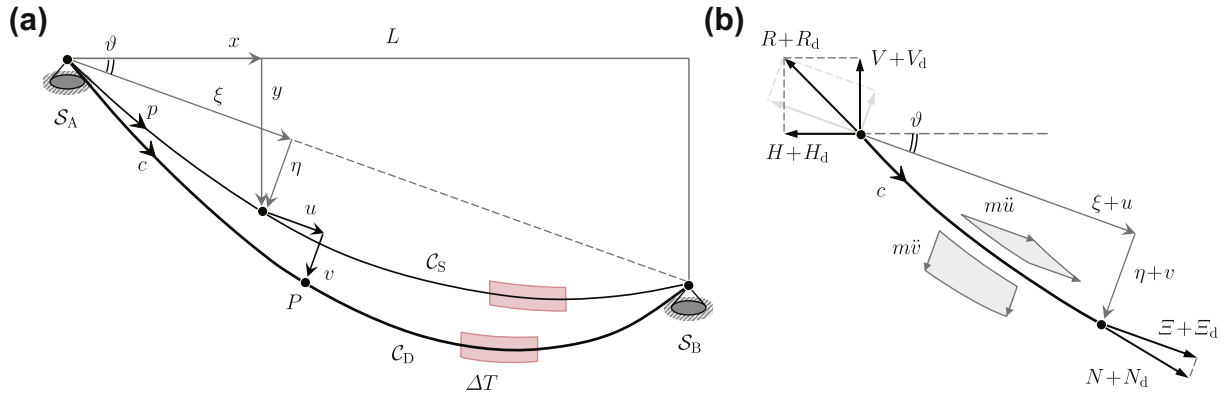

Fig. 4. Planar dynamic response of the inclined suspended cable: (a) components of motion and dynamic configuration $\mathcal{C}_D$ and (b) global dynamic equilibrium.

external forces acting on the cable element. In the local coordinate system they read

$$\frac{\partial}{\partial p}\left[(N+N_d)\left(\frac{d\xi}{dp}+\frac{\partial u}{\partial p}\right)\right]=m\frac{\partial^2 u}{\partial t^2}-w_p\sin(\vartheta) \tag{27}$$

$$\frac{\partial}{\partial p}\left[(N+N_d)\left(\frac{d\eta}{dp}+\frac{\partial v}{\partial p}\right)\right]=m\frac{\partial^2 v}{\partial t^2}-w_p\cos(\vartheta) \tag{28}$$

where m is the uniform mass density per unit strained length in the reference static configuration (that is $mg=w_p$), while N_d, function of both position and time, is the additional dynamic tension.

Expanding and subtracting statically equilibrated terms, and therefore employing the chain rule to the derivatives, the equations of motion become

$$\frac{\partial}{\partial\xi}\left[\Xi\frac{\partial u}{\partial\xi}+\Xi_d\left(1+\frac{\partial u}{\partial\xi}\right)\frac{d\xi}{dp}\right]\frac{d\xi}{dp}=m\frac{\partial^2 u}{\partial t^2}, \tag{29}$$

$$\frac{\partial}{\partial\xi}\left[\Xi\frac{\partial v}{\partial\xi}+\Xi_d\left(\frac{d\eta}{d\xi}+\frac{\partial v}{\partial\xi}\right)\frac{d\xi}{dp}\right]\frac{d\xi}{dp}=m\frac{\partial^2 v}{\partial t^2} \tag{30}$$

where $\Xi=N\mathrm{d}\xi/\mathrm{d}p$ and $\Xi_d=N_d\mathrm{d}\xi/\mathrm{d}p$ represent the chordwise components of the static and additional dynamic tensions, respectively (Fig. 4b). The coupled system of nonlinear partial differential Eqs. (29) and (30), equipped with homogeneous boundary conditions, governs the cable free undamped vibrations.

2.1.1. Static condensation

Within the low-frequency vibration range, it is generally acceptable to formulate the hypothesis of quasi-static stretching, which requires a low longitudinal-to-transversal stiffness ratio (say $H/EA=\mathcal{O}(\epsilon^2)$), and in shallow cables entails negligible chordwise inertia forces in the dominant transversal oscillations. Under this assumption, noting that $\Xi=H_*+\mathcal{O}(\epsilon)$ and then neglecting $\mathcal{O}(\epsilon^3)$-terms, Eq. (29) states

$$\frac{\partial}{\partial\xi}\left(\Xi_d\frac{d\xi}{dp}\right)=0 \tag{31}$$

which means that the quantity between brackets, which has no immediate physical interpretation, does not vary with the chordwise abscissa, and therefore can be assessed as a function of time only

$$\Xi_d\frac{d\xi}{dp}=EAe(t) \tag{32}$$

where the time-dependent function $e(t)$ is often denoted as the dynamic cable *elongation*.

After simple derivative algebra, verifying that the derivative $\mathrm{d}\xi/\mathrm{d}p=1+\mathcal{O}(\epsilon^2)$ and the chordwise component of the static tension $\Xi=H_*(1+\mathrm{d}\eta/\mathrm{d}\xi\tan(\vartheta))+\mathcal{O}(\epsilon^2)$ according to the variable ordering, and finally introducing the cable elongation, Eq. (30) reads

$$H_*\left[\frac{\partial^2 v}{\partial\xi^2}+\frac{\partial}{\partial\xi}\left(\frac{d\eta}{d\xi}\frac{\partial v}{\partial\xi}\right)\tan(\vartheta)\right]+EAe(t)\left(\frac{d^2\eta}{d\xi^2}+\frac{\partial^2 v}{\partial\xi^2}\right)=m\frac{\partial^2 v}{\partial t^2} \tag{33}$$

where, since terms higher than $\mathcal{O}(\epsilon^3)$ have been neglected, an $\mathcal{O}(\epsilon^2)$-approximation of the function $e(t)$ in terms of displacements is required for consistency, while the second term in squared brackets turns out to be certainly negligible for technically-realistic chord inclinations (say $\tan(\vartheta)\leqslant\mathcal{O}(1)$).

Introducing the constitutive relation $N_d=EA\varepsilon_d$ and recalling Eq. (32), the cable elongation can be immediately related to the dynamic extensional strain $\varepsilon_d=\mathrm{d}c/\mathrm{d}p-1$ through the relation

$$e(t)=\varepsilon_d\left(\frac{d\xi}{dp}\right)^2 \tag{34}$$

where, to obtain the required $\mathcal{O}(\epsilon^2)$-approximation, the extensional strain can be expressed as

$$\varepsilon_d=\frac{d\xi}{dp}\left[\frac{\partial u}{\partial\xi}+\frac{d\eta}{d\xi}\frac{\partial v}{\partial\xi}+\frac{1}{2}\left(\frac{\partial v}{\partial\xi}\right)^2\right] \tag{35}$$

and therefore, substituting and integrating for homogeneous boundary conditions, the cable elongation is

$$e(t)=\frac{1}{L_{e*}}\left[\int_{L_*}\frac{d\eta}{d\xi}\frac{\partial v}{\partial\xi}d\xi+\frac{1}{2}\int_{L_*}\left(\frac{\partial v}{\partial\xi}\right)^2 d\xi\right] \tag{36}$$

where L_{e*} is the modified length already defined in (24).

In virtue of static condensation of the longitudinal variable of motion, the cable planar dynamics is finally governed by the nonlinear integral–differential Eq. (33), with partial derivatives in the transversal variable only, equipped with homogeneous boundary conditions. The temperature effects act on the equation coefficients, depending on the static tension and the static configuration derivatives.

Denoting ω_1 as the first circular frequency of the cable at the reference temperature, a suitable nondimensional form of the dynamic equations is introduced through the following variables and parameters

$$\tilde{u}=\frac{u}{L_*},\quad \tilde{v}=\frac{v}{L_*},\quad \tau=\omega_1 t,\quad \gamma^2=\omega_1^2\frac{mL_*^2}{H_*} \tag{37}$$

where γ can be interpreted as the ratio between ω_1 and the first frequency of the taut string with equal elasto-geometrical characteristics ($\gamma>1$). Employing nondimensional variables, Eq. (33) reads

$$\gamma^2\ddot{v} - \left[v'' + (\eta' v')' \tan(\vartheta)\right] - \mu(\eta'' + v'')e(\tau) = 0 \tag{38}$$

and the nondimensional form of the dynamic elongation is

$$e(\tau) = \Lambda_e\left[\int_0^1 \eta' v' \mathrm{d}\xi + \frac{1}{2}\int_0^1 (v')^2 \mathrm{d}\xi\right] \tag{39}$$

where the tilde has been omitted, while dot and apex denote differentiation with respect to the nondimensional time and abscissa, respectively.

2.2. Modal analysis

The integral–differential equation of motion (38) can be linearized around the reference static configuration to study the small amplitude range of transversal oscillations. Considering inclined cables with realistic chord inclinations, the linearized equation reads

$$\gamma^2\ddot{v} - v'' = \mu\eta''\Lambda_e\int_0^1 \eta' v' \mathrm{d}\xi \tag{40}$$

and can be tackled with the separation-of-variables method to calculate the cable frequencies and modes.

Since the thermal effects on the cable dynamics essentially depend on how the temperature modifies the static problem solution, in the dynamic problem the reference static configuration at the generic temperature T, mapped by the polynomial function (22) in shallow cables, can be conveniently expressed as a modification of the configuration at temperature T_0. Considering the cable characteristic parameters (γ^2 and λ^2) referred to temperature T_0, the synthetic factors χ^2 and κ^2 are sufficient to account for the temperature change in the linearized equation of motion

$$\gamma^2\ddot{v} - \chi^2 v'' = -\kappa^4\lambda^2 f\int_0^1 f v \mathrm{d}\xi \tag{41}$$

where, depending on whether the sag-to-chord ratio δ_p, or alternately the inclination angle ϑ, is sufficiently small for the cubic term in Eq. (22) to be neglected (parabolic cables) or not (cubic cables)

$$\text{i.parabolic cables}: \quad f = 1 \tag{42}$$

$$\text{ii.cubic cables}: \quad f = 1 - 8\kappa^2\delta_p(1-2\xi)\tan(\vartheta) \tag{43}$$

that is, the right-hand term of Eq. (41) is constant for parabolic cables.

Following the Irvine solution scheme for shallow parabolic cables (Irvine and Caughey, 1974; Irvine, 1978), the modal problem can be solved in a closed-form fashion. Otherwise, the modal properties of shallow cubic cables can be determined in an approximate way, according to the Rayleigh–Ritz technique.

2.2.1. Closed form solution

Defining $\tilde{\omega}$ as the ratio between the generic frequency ω of the cable at temperature T and the first frequency ω_1 of the cable at the reference temperature T_0, the solution is assumed

$$v(\xi,\tau) = \mathrm{e}^{\mathrm{i}\tilde{\omega}\tau}\phi(\xi) \tag{44}$$

where i denotes the imaginary unit. Replacing the assumed solution in Eq. (40) and eliminating the dependence on time, an ordinary differential equation in the only spatial variable $\phi(\xi)$ is obtained

$$\chi^2\phi'' + \beta^2\phi = k \tag{45}$$

where the coefficient $\beta = \gamma\tilde{\omega}$, and the left-hand integral term is constant for parabolic cables

$$k = \kappa^4\lambda^2\int_0^1\left(\frac{1}{2} - \xi\right)\phi' \mathrm{d}\xi \tag{46}$$

and can be demonstrated to identically vanish for spatially anti-symmetric functions $\phi(\xi)$.

Eq. (45) represents an integral–differential eigenproblem in the unknown eigenfunctions $\phi(\xi)$ and eigenfrequencies β of the cable. For symmetric eigenfunctions the closed-form problem solution follows from the superposition of the homogeneous and the particular solutions

$$\phi(\xi) = C_1\cos\left(\frac{\beta}{\chi}\xi\right) + C_2\sin\left(\frac{\beta}{\chi}\xi\right) + \frac{k}{\beta^2} \tag{47}$$

where from recursive substitution and subsequent integration, the constant k results

$$k = -\frac{\lambda^2\kappa^4}{2\beta}\left[(C_1\beta + 2C_2\chi)\cos\left(\frac{\beta}{\chi}\right) + (C_2\beta - 2C_1\chi)\sin\left(\frac{\beta}{\chi}\right) + C_1\beta - 2C_2\chi\right] \tag{48}$$

otherwise, for anti-symmetric eigenfunctions, the solution falls down into the homogeneous one ($k = 0$).

The eigenproblem is completely solved by imposing the homogeneous boundary conditions, sufficient to determine the eigenfrequencies β and the ratio between the unknown coefficients C_1 and C_2. Then, the corresponding cable circular frequencies are obtained as $\omega = \gamma\omega_1\beta$. Nevertheless, a distinction should be made between anti-symmetric and symmetric eigenfunctions.

2.2.1.1. Anti-symmetric modes. Employing the boundary conditions, it is straightforward to verify that the anti-symmetric cable eigenfunctions present equispaced frequencies, which are integer multiples of the product $2\pi\chi$. Thus explicit expression for the ith frequency can be given

$$\frac{\beta_i}{\chi} = 2\mathrm{i}\pi \quad \mathrm{i} \in \mathbb{N}^+ \tag{49}$$

with corresponding ith modal shape

$$\phi_i(\xi) = C_2\sin\left(\frac{\beta_i}{\chi}\xi\right) \tag{50}$$

where C_2 remains to play the role of indeterminate modal amplitude.

2.2.1.2. Symmetric modes. In contrast, assuming symmetric cable eigenfunction $\phi(\xi)$, and employing the boundary conditions, other cable frequencies born from the roots of the characteristic equation

$$\frac{\beta}{2\chi} - \tan\left(\frac{\beta}{2\chi}\right) = \frac{4}{\lambda_{eq}^2}\left(\frac{\beta}{2\chi}\right)^3, \quad \text{where } \lambda_{eq}^2 = \lambda^2\frac{\kappa^4}{\chi^2} \tag{51}$$

and the modal shape corresponding to the ith frequency β_i is

$$\phi_i(\xi) = C_1\cos\left(\frac{\beta_i}{\chi}\xi\right) + C_2\sin\left(\frac{\beta_i}{\chi}\xi\right) - C_1 \tag{52}$$

where the relation

$$\frac{C_2}{C_1} = \frac{\left(\frac{\beta}{\chi}\right)^3 + \lambda_{eq}^2\left\{\sin\left(\frac{\beta}{\chi}\right) - \frac{\beta}{2\chi}\left[1 + \cos\left(\frac{\beta}{\chi}\right)\right]\right\}}{\lambda_{eq}^2\left\{\frac{\beta}{2\chi}\sin\left(\frac{\beta}{\chi}\right) - \left[1 - \cos\left(\frac{\beta}{\chi}\right)\right]\right\}} \tag{53}$$

subsists between the coefficients.

Fig. 5a shows the frequency loci curves versus the Irvine parameter λ^2. The well-known Irvine diagram is recovered by letting the temperature change vanish (black lines). The diagram presents λ^2-independent frequencies corresponding to fixed anti-symmetric modal shapes, while the frequencies of symmetric modes monotonically increase, with horizontal asymptotic behavior for limit λ^2-values. Thus, greater Irvine parameters correspond to stiffer

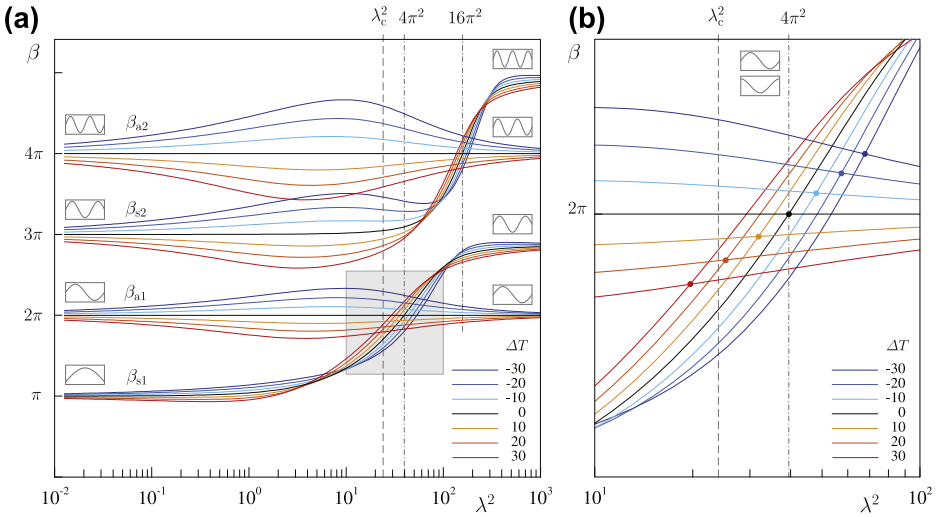

Fig. 5. Frequency loci versus the Irvine parameter: (a) loci of the lowest symmetric (β_{si}) and anti-symmetric (β_{ai}) frequencies for different temperature changes ΔT (with $\alpha = 10^{-5}$) in parabolic cables with $\varrho = 2 \times 10^{-5}$ and (b) window around the crossover between the first (symmetric) and second (first anti-symmetric) frequency.

symmetric modes, which also progressively modify their modal shape. The critical points in which the ramping curves related to the frequency loci of symmetric modes cross the horizontal lines related to the frequency loci of the anti-symmetric modes are called *crossovers* (Fig. 5b). They correspond to internally resonant cables, with two coincident frequencies related to a couple of symmetric and anti-symmetric modes.

2.2.2. Rayleigh–Ritz solution

When the assumption of parabolic static profile cannot be accepted, the modal problem can be tackled according to the Rayleigh–Ritz technique, decomposing the solution according to

$$v(\xi,\tau) = \sum_i q_i(\tau)\psi_i(\xi) \tag{54}$$

where $\psi_i(\xi)$ (with $i = 1,\dots,m$) is a complete set of linearly independent and differentiable trial functions, satisfying the geometric boundary conditions and parametrized by the amplitude $q_i(\tau)$.

Invoking the *virtual work principle* for deformable bodies, where the test function δv is employed as virtual displacement field, the following relation holds between the internal and external virtual works

$$\gamma^2 \int_0^1 \ddot{v}\delta v \mathrm{d}\xi - \chi^2 \int_0^1 v''\delta v \mathrm{d}\xi + \kappa^4\lambda^2 \int_0^1 f v \mathrm{d}\xi \int_0^1 f\delta v \mathrm{d}\xi = 0, \quad \forall \delta v \tag{55}$$

Integrating by parts and introducing the assumed solution for the real and virtual displacement field, a finite-dimensional equation in the amplitude vector $\mathbf{q} = \{q_1,\dots,q_m\}^\top$ is obtained

$$\gamma^2 \delta\mathbf{q}^\top \mathbf{M}\ddot{\mathbf{q}} + \delta\mathbf{q}^\top \mathbf{K}\mathbf{q} = \mathbf{0}, \quad \forall \delta\mathbf{q} \tag{56}$$

where the coefficients of the m-by-m mass matrix $\mathbf{M}$ and stiffness matrix $\mathbf{K}$ are

$$\begin{aligned} M_{ij} &= \int_0^1 (\psi_i\psi_j)\mathrm{d}\xi, \\ K_{ij} &= \chi^2 \int_0^1 \left(\psi_i'\psi_j'\right)\mathrm{d}\xi + \kappa^4\lambda^2 \int_0^1 (f\psi_i)\mathrm{d}\xi \int_0^1 (f\psi_j)\mathrm{d}\xi \end{aligned} \tag{57}$$

Therefore, assuming a harmonic solution for the time-dependent variables $\mathbf{q}(\tau) = \mathbf{c}e^{i\bar{\omega}\tau}$, the resulting eigenvalue problem can be solved in the unknown eigenvalues β_i^2 and eigenvectors $\mathbf{b}_i = \{b_{i1},\dots,b_{im}\}^\top$, giving an approximation of the cable exact frequencies and eigenfunctions $\phi_i(\xi)$, through the superposition

$$\phi_i(\xi) = \sum_j b_{ij}\psi_j(\xi) \tag{58}$$

with the error reducing for an increasing number of trial functions. Given the structure of the problem, no particular symmetry conditions are expected for the eigenfunctions.

In particular, the Rayleigh–Ritz solution is essential to describe the modal properties which characterize the internally-resonant cubic cables (Srinil et al., 2007). Like many other structural systems with crossing frequency loci, suspended cables may exhibit strong frequency and mode sensitivity to small perturbations of the model geometric symmetry in the resonance regions. In particular, it is well known in the scientific literature (Triantafyllou, 1894; Srinil et al., 2007) that the symmetry-breaking effect of the chord inclination can produce a strong, even if extremely localized, interaction between the cable resonant frequencies, whose loci curves approach each other up to a minimum distance, and then suddenly diverge, missing the crossing. This phenomenon is known as (geometric) *frequency veering*, and induces a hybridization process of the involved modes, which exchange their modal shapes in a rapid but continuous way.

2.3. Temperature effects

2.3.1. Parabolic cables

The exact solution of the modal problem for parabolic cables can be verified to recover the Irvine solution as the temperature change vanishes. Moreover, since temperature changes do not modify the formal structure of the modal problem, the comparison with the Irvine solution immediately evidences that the temperature affects the cable frequencies and modes in two different ways, which can be referred to as the *geometric* and *static* effect, respectively. They directly follow from the different thermal effects acting on the static problem solution, and can be interpreted therefrom

- the geometric effect depends on the thermal variation of the static axial tension, which modifies the cable geometric stiffness. From the analytical viewpoint, the geometric effect is responsible for the χ-multiplier affecting the frequencies of both symmetric and anti-symmetric modes.

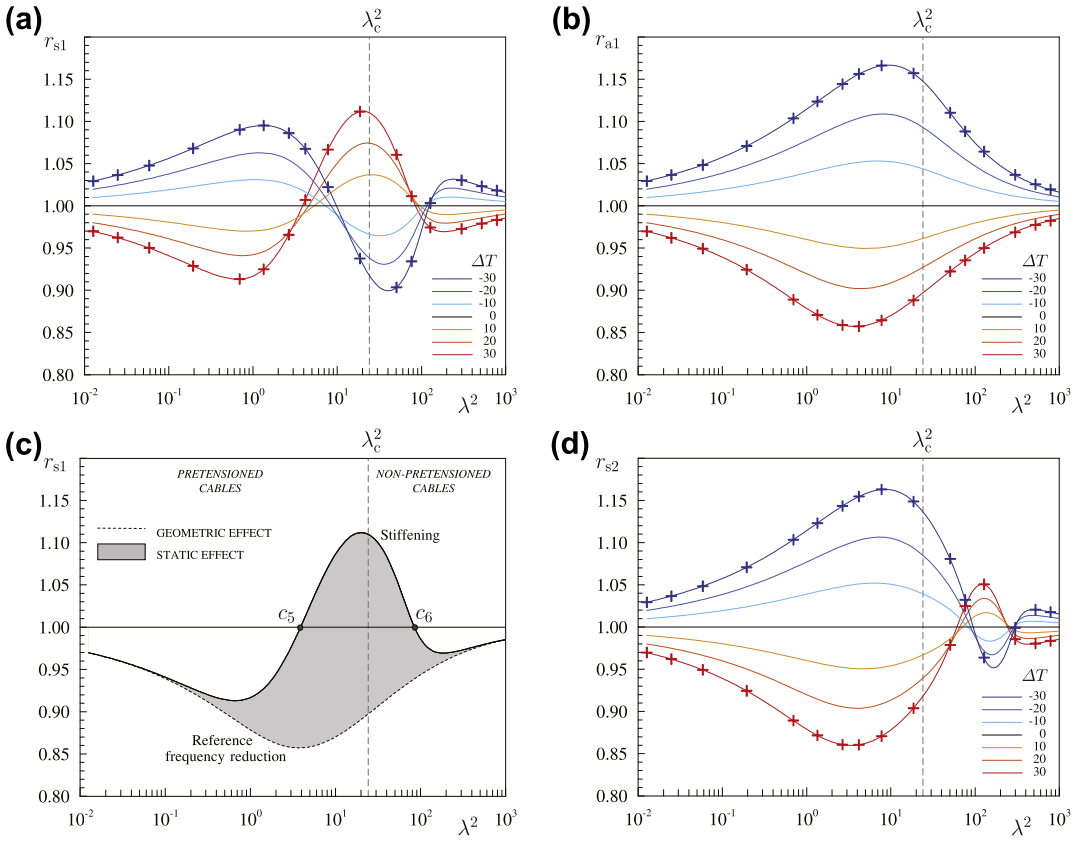

Fig. 6. Frequency ratio versus the Irvine parameter for different temperature changes ΔT (with $\alpha = 10^{-5}$) in parabolic cables with $\varrho = 2 \times 10^{-5}$: (a), (c) first symmetric mode, (b) first anti-symmetric mode and (d) second symmetric mode.

- the static effect depends on the thermal variation of the cable static profile, which in particular modifies the sag and the curvature of the reference configuration. From the analytical viewpoint, the static effect is responsible for the equivalent value λ_{eq}^2 assumed by the Irvine parameter in the characteristic Eq. (51), affecting the frequencies of symmetric modes only.

Despite the two effects not being fully indepedent of each other, since the static effect itself partially depends on the reduced geometric stiffness, their adoption criterion simplifies the physical interpretation of the thermal effects on the modal solution. More rigorously, it could be said that the geometric effect has a secondary consequence on the cable spectrum, since it also partially contributes to the static effect.

Beside the differences related to the symmetry/anti-symmetry of each mode, cables exhibit different sensitivity to the geometric or static effect, depending on the Irvine parameter. Fig. 5a illustrates how different temperature changes modify the Irvine diagram. To better evidence the temperature effects on each cable frequency it is useful to introduce the ratio $r_i = \beta_i/\beta_{i0}$, where β_{i0} is the ith frequency at the reference temperature. It is convenient to separately discuss the frequency ratio of the lowest symmetric modes ($r_{s1,s2}$ in Fig. 6a and d), affected by both the geometric and static effect, and the first anti-symmetric mode (r_{a1} in Fig. 6b), affected by the geometric effect only

i. considering the frequency ratio r_{a1} of the anti-symmetric mode for temperature increments ($\Delta T > 0$, red[1] curves in Fig. 6b), the geometric effect determines a systematic frequency reduction ($r_{a1} < 1$) in the whole range of the Irvine parameter λ^2. Opposite temperature changes ($\Delta T < 0$, blue curves) determine a systematic frequency increment ($r_{a1} > 1$). All the r_{a1}-curves present horizontal asymptotes for limiting λ^2-values, and are characterized by a maximum (or a minimum, depending on the temperature change sign) close to the critical value λ_c^2. The same curves are also representative of the frequency ratio for all the higher anti-symmetric modes;

ii. considering the frequency ratio r_{s1} of the lowest symmetric mode for temperature increments ($\Delta T > 0$, red curves in Fig. 6a), the geometric and the static effect act simultaneously. Selecting a certain temperature change ($\Delta T = 30$), the two effects can be conveniently separated (Fig. 6c). The geometric effect is found to determine a systematic frequency reduction (dashed line), identical to that affecting anti-symmetric modes, in the whole λ^2-range. Taking this frequency reduction as a reference, the static effect applies a stiffening action (upward gray shift). Globally, the geometric effect is dominant for high or low λ^2-values (approximately for $\lambda^2 < 1$, or $\lambda^2 > 100$), whereas the static effect becomes gradually relevant over a wide λ^2-range (say for $1 < \lambda^2 < 100$) and ends up prevailing, causing a frequency increment ($r_{s1} > 1$), around the critical value λ_c^2. As a minor remark, for each temperature change, the perfect balance of the geometric and static effect ($r_{s1} = 1$) is realized for a pair of λ^2-values (points c_5 and c_6). If the temperature change sign is inverted ($\Delta T < 0$, blue curves), the geometric and static effect simultaneously apply a frequency increment and softening action, respectively, whose competition determines a similar, but opposite scenario.

[1] For interpretation of color in Figs. 3 and 6, the reader is referred to the web version of this article.

Table 1
Thermal effects of the cable frequencies.

	ANTI-SYMMETRIC MODE FREQUENCIES (geometric effect only)	i-th SYMMETRIC MODE FREQUENCY (geometric and static effect)		
WARNING ($\Delta T>0$)	REDUCTION ($r_{\mathrm{a}}<1$)	REDUCTION ($r_{\mathrm{si}}<1$)	INCREMENT ($r_{\mathrm{si}}>1$)	REDUCTION ($r_{\mathrm{si}}<1$)
COOLING ($\Delta T<0$)	INCREMENT ($r_{\mathrm{a}}>1$)	INCREMENT ($r_{\mathrm{si}}>1$)	REDUCTION ($r_{\mathrm{si}}<1$)	INCREMENT ($r_{\mathrm{si}}>1$)
	$\lambda^2 \ll 1$ ... $\lambda^2 \gg 1$	$\lambda^2 \ll 1$ ... $\lambda^2 = 4\mathrm{i}^2\pi^2\chi^2/\kappa^4$ ... $\lambda^2 \gg 1$		

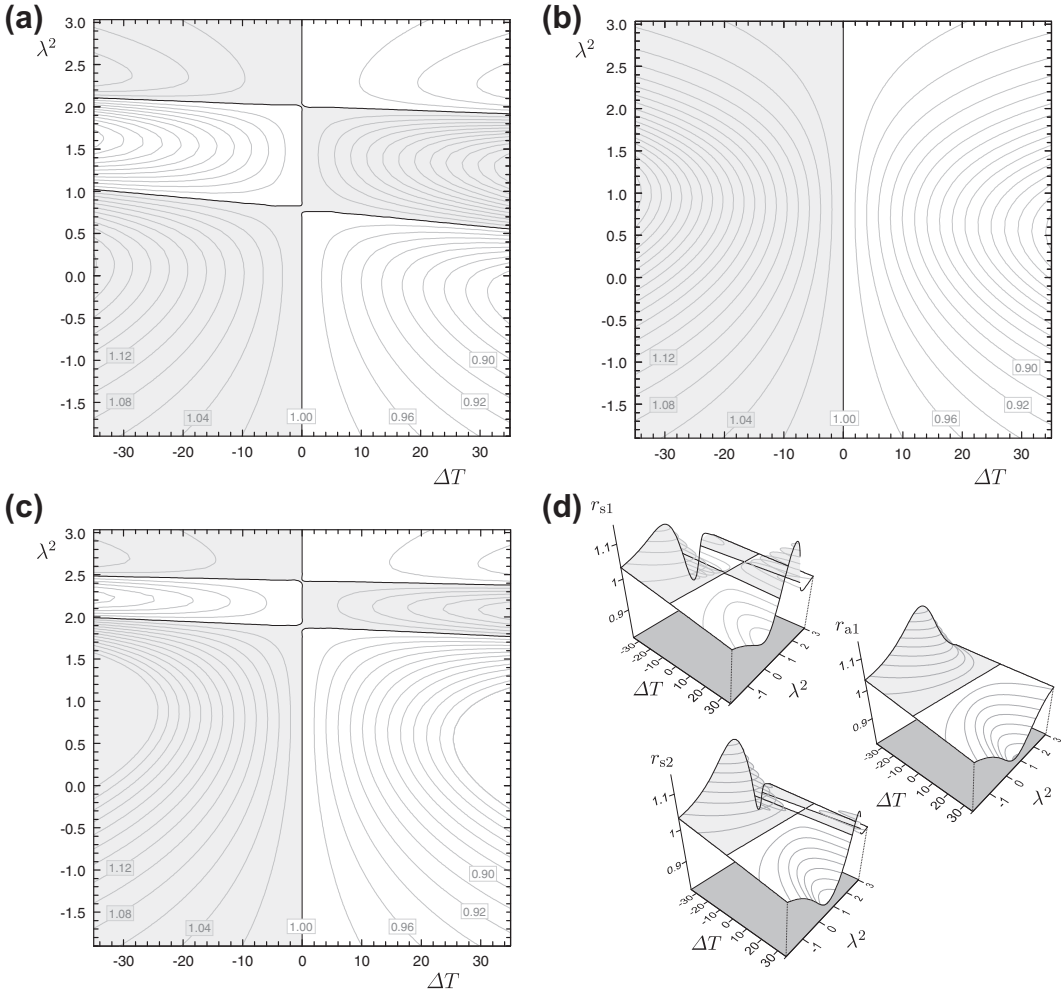

Fig. 7. Frequency ratio for parabolic cables (with $\varrho = 2 \times 10^{-5}, \alpha = 10^{-5}$) in the ΔT-λ^2 plane (logarithmic scale for λ^2): (a) frequency ratio r_{s1} of the first symmetric mode, (b) frequency ratio r_{a1} of the first anti-symmetric mode, (c) frequency ratio r_{s2} of the second symmetric mode and (d) 3D view.

The different behavior of symmetric and anti-symmetric modes, depending on the Irvine parameter, can be synthesized in the scheme of Table 1. In Fig. 6, the analytical findings are optimally confirmed by a set of numerical results, marked by the crosses, obtained from finite element models. The contour plot of the r_i-manifolds in the ΔT–λ^2 plane, shown in Fig. 7, clearly evidences that the thermal effects on the linear frequencies are not exactly symmetric with respect to the reference temperature.

Combining the physical interpretation of the temperature effects and the parametric analysis results yields some observations worthy of summarization. A warming temperature change certainly softens the cable transversal vibrations, as a consequence of the minor geometric stiffness caused by the static tension loss (geometric effect). Nonetheless, the symmetric component of the transversal vibrations is unavoidably subject to a competing stiffening action, consequent to the major cable sag, or curvature,

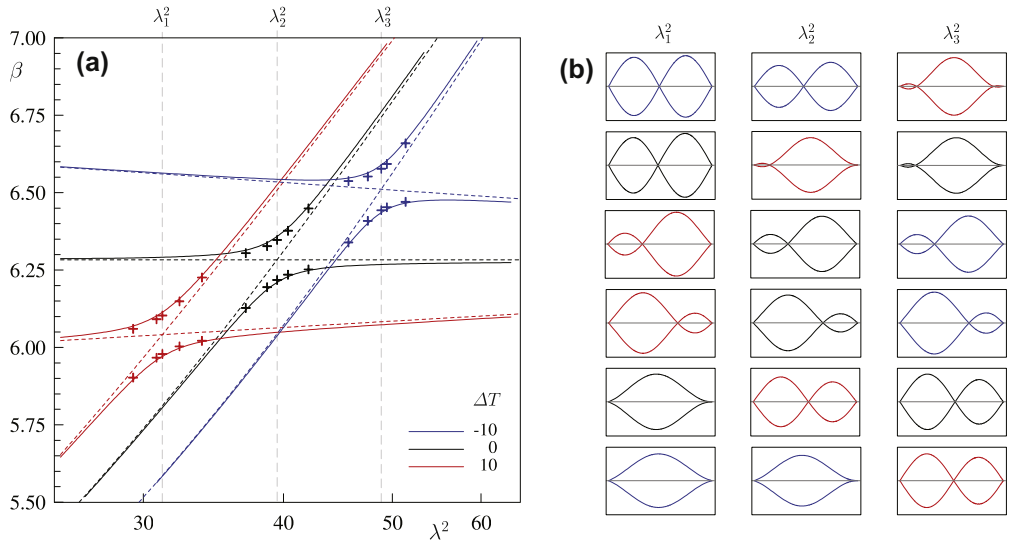

Fig. 8. Frequency loci versus the Irvine parameter for cubic cables ($\varrho = 2 \times 10^{-5}$, $\alpha = 10^{-5}$) with chord inclination $\vartheta = \pi/6$: (a) first symmetric and anti-symmetric mode in the frequency veering region and (b) hybridization of the modal shapes.

caused by the amplification of the static equilibrium profile (static effect). Therefore, warming temperature changes do not necessarily imply a reduction of all the cable frequencies (see the gray regions in Fig. 7 in the right semi-plane). The Irvine parameter is sufficient to determine which of the competing effects prevails for a certain cable. Independently of the vibration frequency, strongly pretensioned taut cables ($\lambda^2 \ll 1$) and non-pretensioned slack cables ($\lambda^2 \gg 1$) tend to be less sensitive to temperature, and to the static effect in particular. Cables with natural length close to the distance between the supports ($\lambda^2 \simeq \lambda_c^2$) are the most sensitive to the geometric effect. On the contrary, the cable sensitivity to the static effect is different for each symmetric mode. Indeed, since the static effect acts as an apparent modification of the Irvine parameter, the region dominated by the static effect is limited to the λ^2-range corresponding to the ramping portion of the each frequency loci curve in the Irvine diagram (see Fig. 5a). Within this region, which is different for each symmetric mode, the higher apparent values of the Irvine parameter accelerate the rate of frequency increase. Therefore, the stiffening action of the static effect is justified by the shift of the frequency loci ramping, which in warmed cables correspond to lower Irvine parameters. As a minor remark, this effect determines also a leftward shift of the frequency cross-over points (Fig. 5b). Coherent with these arguments, in higher symmetric modes the relevant range of the static effect moves towards greater λ^2-values (see r_{s2} in Fig. 6d).

Finally, only minor qualitative thermal effects can be observed on the modal shapes from the comparison with cables at the reference temperature. Particularly, temperature changes do not modify the anti-symmetric modes, since they are independent of the cable sag, and thus are not sensitive to the static effect. Moreover, since the anti-symmetric modal shapes do not involve cable stretching, they are even not sensitive to the geometric effect due to the reduction of axial stiffness. In contrast, a certain sensitivity of the symmetric modes to the static effect can be appreciated. Indeed the apparent modification of the Irvine parameter may slightly anticipate or delay, depending on the temperature change sign, the shape transformation of symmetric modes accompanying the ramping part of the related frequency loci curve.

According to the work motivations, it may be interesting to remark that temperature changes may determine frequency variations qualitatively and quantitatively similar to those affecting a cable damaged by a diffused reduction of the axial stiffness (Lepidi et al., 2007). Analogies or differences among the temperature and damage effects on the cable modal properties, together with a discussion of the potential impact of thermal changes on frequency-based damage identification procedures can be found in Lepidi (2011).

2.3.2. Cubic cables

The temperature-dependent crossover points characterizing the perfect internal resonance between the *i*th pair of symmetric and anti-symmetric modes in parabolic cables can be easily located in the Irvine diagram, since the corresponding critical λ^2-values can be exactly determined

$$\lambda_{cr}^2 = 4i^2\pi^2\frac{\chi^2}{\kappa^4} \tag{59}$$

This resonance condition, at each environmental temperature, has some importance because of the significant flows of mechanical energy which can be exchanged by the resonant modes. When cubic cables are considered, similar interest may be generated by the thermal effects on the quasi-resonance condition determined by the frequency veering. Fig. 8 shows the frequency veering curves at different temperatures for a selected cable inclination ($\vartheta = \pi/6$), obtained using ten Rayleigh–Ritz test functions. Despite the translation of the underlying crossover points, it can be clearly observed that the veering phenomenon is almost identically preserved for temperature changes. In particular, the minor thermal effects on the symmetry loss in cubic cables are not sufficient to significantly modify the veering amplitude, which depends only on the cable inclination, and remains practically unchanged for both temperature increment and reduction. The analytical findings are confirmed with satisfying agreement, despite a slight underestimation of the veering amplitude, by a set of finite element results, marked by the crosses.

3. Conclusions

A continuous monodimensional model has been presented to describe the mechanical behavior of an elastic suspended cable under uniform thermal load. The environmental temperature change is introduced through a non-homogeneous constitutive law for the material linear elasticity. The equations governing the static prob-

lem, for generic inclination of the chord between the supports, are solved to achieve the exact cable equilibrium configuration under self-weight. Temperature changes determine an opposite-sign variation of the static tension and sag, which is evaluated by synthetic factors defined to the purpose. The significance of each of these two thermal effects, which are however not independent, is parametrically investigated. Qualitatively, their importance monotonically builds up for increasing temperature changes in the whole space of elastic and geometric properties. Quantitatively, cables with natural length close to the distance between the supports reveal the highest sensitivity to temperature, whereas pretensioned and non-pretensioned cables are gradually less sensitive to thermal effects.

The nonlinear equations governing the planar finite motions of the cable around the static configuration have also been presented. The closed-form solution for the spectral properties characterizing the low-frequency free undamped dynamics of shallow parabolic cables is obtained, considering a quasistatic treatment of the longitudinal component of motion. Under this simplifying assumption, two simultaneous temperature effects have been recognized. The first one, namely the *geometric effect*, is related to the geometric stiffness variation, following from the varied static tension, and produces a systematic increment or reduction of the cable frequencies, for both the anti-symmetric and symmetric modes, in the whole Irvine parameter range. The second one, namely the *static effect*, is due to the varied sagging static profile, and acts as an apparent modification of the cable Irvine parameter. Competing with the simultaneous geometric effect, the static effect stiffens or softens only the symmetric modes, and ends up prevailing over a large range of the Irvine parameter, different for each symmetric mode. Temperature changes determine also a slight shift of the crossover points, corresponding to perfect internal resonances between a pair of symmetric and anti-symmetric modes. Thermal effects are proved instead to cause only a minimal modification of the cable modal shapes.

Finally, the symmetry-breaking effect of the chord inclination in the static configuration of shallow cubic cables is analyzed through an approximate solution of the modal problem. Thermal effects are proved to not significantly modify the spectral properties of internally-resonant cubic cable, characterized by the veering of the frequency loci and the hybridization of the modal shapes.

Appendix

The nondimensional auxiliary functions introduced to describe the cable static configuration $\mathcal{C}_S$ read

$$\Psi_1(s) = \operatorname{arcsinh}[\tan(\varphi_A)] - \operatorname{arcsinh}[\tan(\varphi(s))], \tag{60}$$

$$\Psi_2(s) = \left[1+\tan^2(\varphi_A)\right]^{\frac{1}{2}} - \left[1+\tan^2(\varphi(s))\right]^{\frac{1}{2}} \tag{61}$$

for the coordinate functions defined in (6), and

$$\Psi_3(s) = \tan(\varphi_A)\left[1+\tan^2(\varphi_A)\right]^{\frac{1}{2}} - \tan^2(\varphi(s))\left[1+\tan^2(\varphi(s))\right]^{\frac{1}{2}}, \tag{62}$$

$$\Psi_4(s) = \log\left[\tan(\varphi_A) + \left[1+\tan^2(\varphi_A)\right]^{\frac{1}{2}}\right] - \log\left[\tan(\varphi(s)) + \left[1+\tan^2(\varphi(s))\right]^{\frac{1}{2}}\right] \tag{63}$$

for the curvilinear abscissa defined in (8). The relevant trigonometric terms are defined as

$$\tan(\varphi_A) = \frac{V}{H}, \quad \tan(\varphi(s)) = \frac{V - ws}{H} \tag{64}$$

and correspond to the local tangent to the cable static profile at the left support S_A and at the curvilinear abscissa s, respectively.

References

Basseville, M., Bourquin, F., Mevel, L., Nasser, H., Treyssede, F., 2010. Handling the temperature effect in vibration monitoring: two subspace-based analytical approaches. Journal of Engineering Mechanics 136, 367–378.

Caetano, E., Cunha, A., Gattulli, V., Lepidi, M., 2008. Cable-deck dynamic interactions at the international guadiana bridge: on-site measurements and finite element modelling. Structural Control and Health Monitoring 15, 237–264.

Degrauwe, D., De Roeck, G., Lombaert, G., 2009. Uncertainty quantification in the damage assessment of a cable-stayed bridge by means of fuzzy numbers. Computers and Structures 87, 1077–1084.

Deraemaeker, A., Reynders, E., De Roeck, G., Kullaa, J., 2008. Vibration-based structural health monitoring using output-only measurements under changing environment. Mechanical Systems and Signal Processing 22, 34–56.

Gattulli, V., 2007. Advanced Control Strategies in Cable Dynamics. Springer, Stirlingshire, UK, pp. 243–269.

Gattulli, V., Lepidi, M., 2007. Localization and veering in the dynamics of cable-stayed bridges. Computers and Structures 85, 1661–1678.

Irvine, H., 1978. Free vibrations of inclined cables. Journal of the Structural Division 104, 343–347.

Irvine, H., 1981. Cable Structures. MIT Press Series in Structural Mechanics. MIT Press.

Irvine, H., Caughey, T., 1974. The linear theory of free vibrations of a suspended cable. Royal Society of London Proceedings Series A 341, 299–315.

Irvine, H., Sinclair, G., 1976. The suspended elastic cable under the action of concentrated vertical loads. International Journal of Solids and Structures 12, 309–317.

Lacarbonara, W., Paolone, A., Vestroni, F., 2007. Elastodynamics of nonshallow suspended cables: linear modal properties. Journal of Vibration and Acoustics, Transactions of the ASME 129, 425–433.

Lepidi, M., 2011. Static and dynamic response of elastic suspended cables under diffused damage and uniform thermal load. In: Proceedings of the XX AIMETA Congress, Bologna, Italy.

Lepidi, M., Gattulli, V., 2011. Static and dynamic response of elastic suspended cables under uniform temperature change. Technical Report 1/2011. DISAT – University of L'Aquila.

Lepidi, M., Gattulli, V., Vestroni, F., 2007. Static and dynamic response of elastic suspended cables with damage. International Journal of Solids and Structures 44, 8194–8212.

Macdonald, J., Daniell, W., 2005. Variation of modal parameters of a cable-stayed bridge identified from ambient vibration measurements and fe modelling. Engineering Structures 27, 1916–1930.

Matsumoto, M., Daito, Y., Kanamura, T., Shigemura, Y., Sakuma, S., Ishizaki, H., 1998. Wind-induced vibration of cables of cable-stayed bridges. Journal of Wind Engineering and Industrial Aerodynamics, 1015–1027.

Ni, Y., Hua, X., Fan, K., Ko, J., 2005. Correlating modal properties with temperature using long-term monitoring data and support vector machine technique. Engineering Structures 27, 1762–1773.

Peeters, B., Maeck, J., De Roeck, G., 2001. Vibration-based damage detection in civil engineering: excitation sources and temperature effects. Smart Materials and Structures 10, 518–527.

R&D ADINA, I., 2009. ADINA Theory and Modeling Guides.

Rega, G., 2004. Nonlinear vibrations of suspended cables – Part i: Modeling and analysis, Part ii: Deterministic phenomena. Applied Mechanics Reviews 57, 443–514.

Rega, G., Alaggio, R., 2009. Experimental unfolding of the nonlinear dynamics of a cable-mass suspended system around a divergence-hopf bifurcation. Journal of Sound and Vibration 322, 581–611.

Rega, G., Vestroni, F., Benedettini, F., 1984. Parametric analysis of large amplitude free vibrations of a suspended cable. International Journal of Solids and Structures 20, 95–105.

Srinil, N., Rega, G., Chucheepsakul, S., 2007. Two-to-one resonant multi-modal dynamics of horizontal/inclined cables. Part I: Theoretical formulation and model validation. Nonlinear Dynamics 48, 231–252.

Tabatabai, H., 2005. Inspection and maintenance of bridge stay cable systems: a synthesis of highway practice. NCTRP Synthesis 353, Transportation Research Board, NRC.

Triantafyllou, M.S., 1894. The dynamics of taut inclined cables. Quarterly Journal of Mechanics and Applied Mathematics 37, 421–440.

Wang, X., Wu, Z., 2010. Evaluation of frp and hybrid frp cables for super long-span cable-stayed bridges. Composite Structures 92, 2582–2590.

Yang, D., Youliang, D., Aiqun, L., 2010. Structural condition assessment of long-span suspension bridges using long-term monitoring data. Earthquake Engineering and Engineering Vibration 9, 123–131.

Zhou, H., Ni, Y., Ko, J., 2010. Constructing input to neural networks for modeling temperature-caused modal variability: mean temperatures, effective temperatures, and principal components of temperatures. Engineering Structures 32, 1747–1759.